Noname manuscript No.
(will be inserted by the editor)

A Robot Leg with Compliant Tarsus and its Neural Control for Efficient and Adaptive Locomotion on Complex Terrains

G. Di Canio[1,†] · S. Stoyanov[1,†] · J.C. Larsen[1] · J. Hallam[2] · A. Kovalev[3] · T. Kleinteich[3] · S.N. Gorb[3] · P. Manoonpong[1,*]

Received: date / Accepted: date

Abstract Insects, like dung beetles, show fascinating locomotor abilities. They can use their legs to walk on complex terrains (e.g., rocky and curved surfaces) and to manipulate objects. They also exploit their compliant tarsi, increasing the contact area between the legs and surface, to enhance locomotion and object manipulation efficiency. Besides these biomechanical components, their neural control allows them to move at a proper frequency with respect to their biomechanical properties and to quickly adapt their movements to deal with environmental changes. Realizing these complex achievements on artificial systems remains a grand challenge. As a step towards this direction, we present here our first prototype of an artificial dung beetle-like leg with compliant tarsus by analyzing real dung beetle legs through μCT scans. Compliant tarsus was designed according to the so-called fin ray effect. Real robot experiments show that the leg with compliant tarsus can efficiently move on rocky and curved surfaces. We also apply neural control, based on a central pattern generator (CPG) circuit and synaptic plasticity, to autonomously generate a proper moving frequency of the leg. The controller can also adapt the leg movement to deal with environmental changes, like different treadmill speeds, within a few steps.

Keywords Central pattern generator · Bio-inspired robotics · Neural control · Embodiment · Adaptive locomotion · Dung beetle · Fin ray

1 Introduction

During the last few decades, research in the domain of bio-inspired robotics has tried to imitate natural features of walking animals with artificial legged systems. Examples include the HECTOR robot [1] and the LAURON robot [2] based on the studies of a stick insect, the AMOS robot [3] inspired by a cockroach, the robot BILL-ANT [4] inspired by an ant, just to name a few. Typically, these walking robots as well as many others have the same standard stick insect-like leg structure [5] with a simplified hemispherical foot tip for locomotion. To enhance and expand locomotion ability, some walking robots have been developed with nonstandard foot designs [6], [7], [8], [9], [10].

While all these robots can perform different locomotion modes, like walking on rough terrain [1], [2] and climbing [3], efficient locomotion on complex terrains (e.g., a cylindrical rod/tube [11] as well as a loose rocky surface [3]) with fast adaptation to deal with environmental changes have not been fully realized on an individual legged robot system. Furthermore, if manipulation tasks are required, additional manipulators and/or grippers are usually installed instead of using existing leg structure [4], [12], [13]. This becomes energy inefficient due to added load and the requirement of additional energy to power the manipulator or gripper system. Compared to these solutions, insects with moderate neural computing can use their legs for both locomo-

*E-mail: poma@mmmi.sdu.dk
†These authors contributed equally to this work

[1]Embodied AI & Neurorobotics Lab, Centre for BioRobotics, The Mæsk Mc-Kinney Møller Institute, The University of Southern Denmark, Odense M, DK-5230, Denmark

[2]Centre for BioRobotics, The Mæsk Mc-Kinney Møller Institute, University of Southern Denmark, Odense M, DK-5230, Denmark

[3] Functional Morphology and Biomechanics, Zoological Institute, Kiel University, Kiel, D-24118, Germany

tion as well as object manipulation and transportation. They can efficiently walk on diverse complex terrains (e.g., rocky and curved substrates [14]). For example, dung beetles are able to not only walk but also manipulate and transport an object using some legs [15], [16]. They also exploit their compliant tarsi to increase the contact area between the legs and the substrate. This results in the enhancement of their locomotion and object manipulation efficiency [15], [17]. Inspired by this, we have investigated biomechanical structures of real dung beetle legs and kinematics through μCT [18]. As a first step, this paper presents here 1) a prototype of a hind leg of the beetle for locomotion, 2) bio-inspired compliant tarsus (i.e., robot foot) for contact force reduction and locomotion enhancement on complex terrains, and 3) neural control with synaptic plasticity for fast adaptation allowing the leg to deal with environmental changes. In the following sections, we describe the dung-beetle like leg with the bio-inspired compliant tarsus and its neural control for locomotion and adaptation. Results, including contact force reduction, efficient locomotion on rocky surface and a cylindrical tube, and fast adaptation to deal with the different speeds of a treadmill, are provided alongside the sections from which they mainly derive because this provides a better understanding of their functionalities.

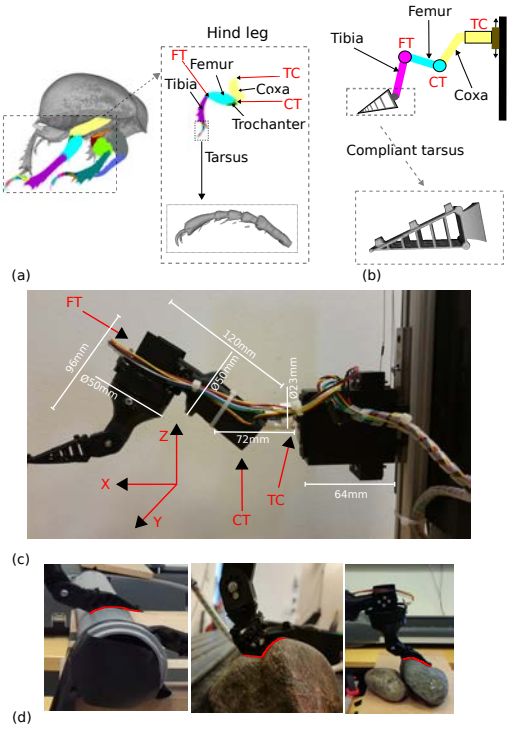

Fig. 1 (a) 3D structure of the dung beetle *Geotrupes stercorarius* (posterio-lateral view). Zoom panel shows the segmented hind leg and tarsus of the beetle. (b) Dung beetle-like hind leg with bio-inspired (fin ray) compliant tarsus. Zoom panel shows the compliant tarsus with a size of 20 mm wide, 20 mm high, and 45 mm long. (c) The setup of the leg with a support. (d) Compliant property of the tarsus allowing it to passively change its shape with respect to different surfaces.

2 Dung beetle-like leg with compliant tarsus

In this study, we first focus on a hind leg of a dung beetle which plays an important role for both locomotion and object manipulation. We analyze the leg by using a desktop μCT scanner (Skyscan 1172) which captures x-ray images over a 360˚rotation of the beetle. Based on these x-ray images, we reconstruct a volumetric 3D dataset that consists of a stack of virtual cross-section images through the entire specimen. Then during post-processing of the μCT data, we interactively segment the parts of the beetle's leg from the dataset by assigning different labels to individual pixels within the stack of cross-sectional images. The segmented structures can then be visualized independently from the remainder μCT dataset (Fig. 1 (a)) and be exported as polygonal surfaces for 3D printing.

As showed in Fig. 1(a), the leg consists of five main segments from the proximal part to the distal part. They are called coxa, trochanter, femur, tibia, and tarsus. There are three main active joints: TC-joint (connecting thorax and coxa), CT-joint (connecting coxa and trochanter), and FT-joint (connecting femur and tibia). Trochanter and femur segments are connected by a joint which allows very small movements and, therefore, can be considered as a fused component. Tarsus is divided into five segments which are connected to each other with flexibility and compliance [14], [19], [20]. According to this, the tarsus can easily change its shape with respect to a substrate on which it makes contact [14]; thereby increasing the contact area between the leg and the substrate for locomotion and object manipulation enhancement. There is pretarsus with a claw-like structure attached to the last part of the tarsus [17].

As a first step, for developing a real dung beetle-like leg, we consider here the three active joints (TC-, CT-, and FT-joints) and the tarsus of the hind leg of the dung beetle. Three segments (coxa, femur, and tibia) between the joints are simplified and designed by following the proportion of the hind leg (i.e., coxa:femur:tibia is 1:1.2:1, see Fig. 1(c)). The lengths of the coxa, femur, and tibia parts are 7 cm, 8.4 cm, and 7 cm, respectively. They are printed using 3D-printing (Fig. 1(c)). For simplification, the CT- and FT-joints rotate around the y-axis while the TC-joint rotates around the x-axis. These rotations follow the joint rotations of the real dung beetle leg. The TC-joint is driven by the Hitec HS645MG servo motor with a maximum torque of 10.0

kg-cm while the CT- and FT-joints are driven by the Hitec HS85MG micro servo motor with a maximum torque of 3.5 kg-cm. The main purpose for using different servo motors is to balance between the torque and length of the segments and to keep the entire leg in a minimal size. A study of dynamic force applied to each leg joint also suggests that the TC-joint supporting the whole body structure requires high torque while the other two joints require smaller torque. Additionally, all these servo motors are modified to obtain potentiometer sensor signals for detecting the actual joint angle positions. The base of the TC-joint is attached to a linear slide allowing the leg to freely move in a vertical direction along the z-axis (Fig. 1(c)). A flexible cable is used to hold the leg during a swing phase for ground clearance. This mimics the action of other legs not represented in the current setup. All servo motors are driven by the output signals of neural control (described below) through the Multi-Servo IO-Board (MBoard). The potentiometer signals are also digitized using this board. The MBoard is interfaced with a personal computer (PC) via an RS232 serial connection at 57.6 kbits per second.

For the tarsus part of the leg, we simplify it by using a fin-ray inspired concept[1] which compliancy mimics the segmented structure of the real tarsus of the beetle. It consists of five rays/blades embedded inside its triangular structure (Fig. 1(b)). Its length is about 5 cm which is proportional to the tarsus of the dung beetle (Fig. 1(a)). It is printed using 3D-printing with a compliant material (i.e., rubber). Although this design does not fully capture the complete complex structure of the tarsus of the dung beetle, it, as an abstract version, shows flexibility and compliance to passively adapt its shape to follow the contour of a substrate (Fig. 1(d)) as observed in the beetle. Besides the passive adaptation, the tarsus design also acts as a damping system to reduce contact force when the leg touches the ground (see below).

Contact force reduction

Here we observe contact force acting on the leg with the bio-inspired tarsus (Fig. 1(c)) for different surfaces and compare it with the forces obtained from a triangular tarsus without rays[2] and a standard hemispherical foot [9]. For this test, we dropped the leg with the different foot structures from a distance of 2 cm above flat and rocky surfaces (Figs. 2(a) and (b), top).

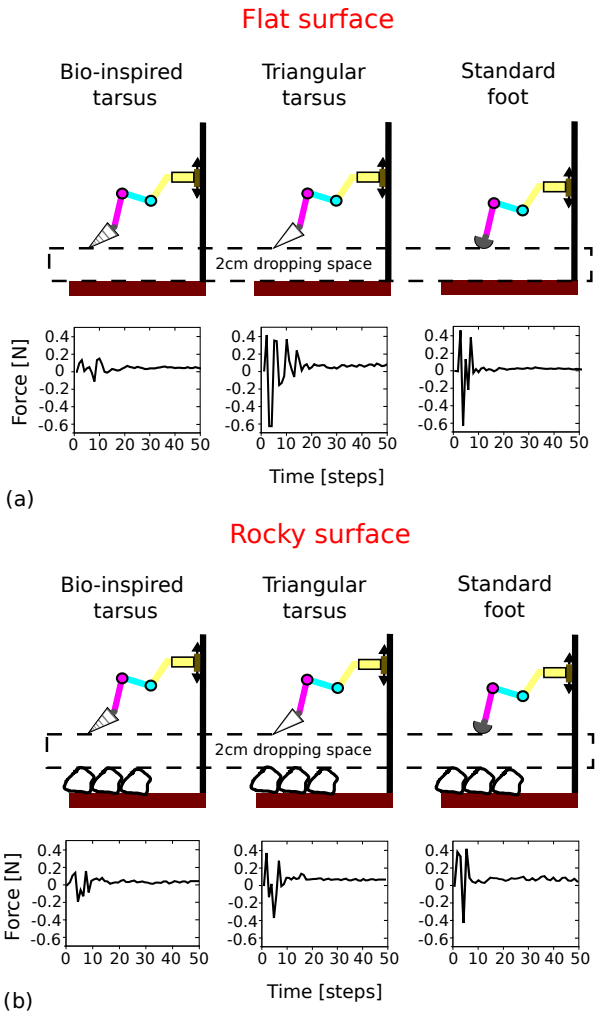

Fig. 2 (a)-top The setup of flat surface experiments. (a)-bottom Force measurement during the flat surface experiments with different foot structures. (b)-top The setup of rocky surface experiments. (b)-bottom Force measurement during the rocky surface experiments with different foot structures.

An accelerometer was installed to measure the acceleration of the leg and to calculate contact force. The results of this test are shown in Figs. 2 and 3. It can be seen that the highest peak of contact force (Figs. 2(a) and (b), bottom) can be significantly reduced when the bio-inspired compliant tarsus is employed. Figure 3 shows average force with 95% confidence interval obtained from five experiments for each foot structure where the bio-inspired tarsus shows the smallest average force values for both surfaces. This test suggests that not only the shape but also the structure of the

[1] Although such a structure has been developed and employed as a gripper of robot arms for object manipulation (see MultiChoiceGripper of Festo at https://www.festo.com/bionik), it is here developed and employed as a robot foot for efficient locomotion.

[2] This tarsus has the same shape and size as the bio-inspired compliant tarsus but it lacks flexibility and compliance due to its structure.

foot are important for the design to obtain flexibility and compliance resulting in contact force reduction. This force reduction avoids a high contact force (or impact force) to the motors and the structure of the leg; thereby preventing damage to the leg.

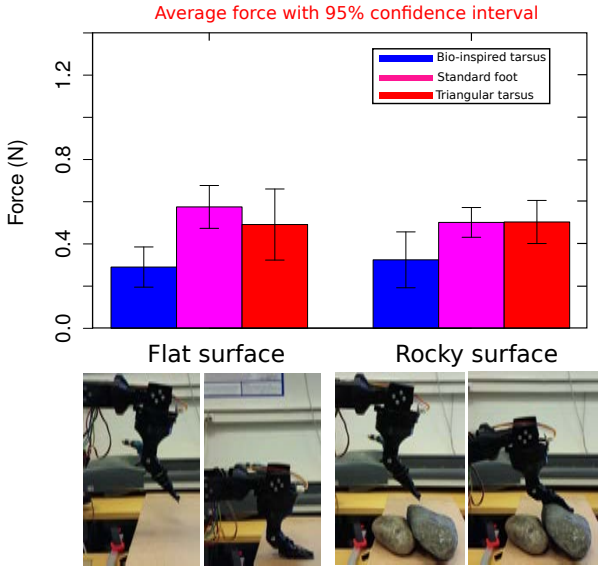

Fig. 3 Average force with 95% confidence interval obtained from five experiments for each foot structure on flat and rocky surfaces. Bottom figures exemplify dropping the leg with the bio-inspired tarsus on the flat and rocky surfaces. The deformation of the tarsus, acting as a damper, can be observed when it touched the surfaces; thereby allowing for contact force reduction. We also encourage readers to watch a slow motion video showing the deformation of the tarsus at http://www.manoonpong.com/DB/S1.mp4.

3 Neural control for locomotion

The concept of central pattern generators (CPGs) for locomotion has been studied and used in several robotic systems of particular walking robots [21]. There is a wide variety of different CPG models available ranging from detailed biophysical models to pure mathematical oscillator models [22], [23], [24]. Here, the model of a CPG for basic locomotion of our dung beetle-like leg is realized by using the discrete-time dynamics of a simple 2-neuron oscillator network [25] (Fig. 4(a)). Due to its neurodynamics, it is able to autonomously generate various periodic and chaotic signals [26] without sensory feedback; i.e., it can act as open-loop control. However, it can be extended by using synaptic plasticity mechanisms allowing it to quickly adapt to the frequency of an external perturbation or sensory feedback (i.e., closed-loop control) and to memorize the influence of the perturbation (see Section 4). These features make the minimal CPG versatile and thereby distinct from other models [22], [23], [24].

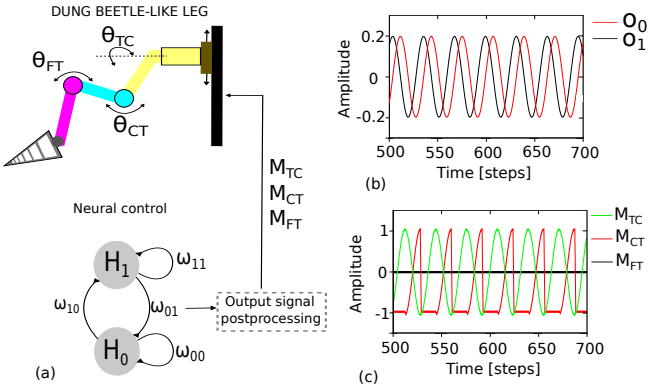

Fig. 4 (a) CPG-based neural control for locomotion. It consists of two interconnected neurons $H_{0,1}$. (b) Outputs $o_{0,1}$ of the neurons $H_{0,1}$ of the CPG-based control. (c) Motor signals $M_{TC,CT,FT}$ obtained from a CPG output signal postprocessing unit. The post processing unit translates the outputs $o_{0,1}$ into the proper motor signals.

For our implementation here, the activity of each neuron develops according to $a_i(t+1) = \sum_{j=1}^{n} W_{ij}\, o_j(t)$; $i = 1, \ldots, n$ with an update frequency of 20 Hz, where n denotes the number of units. The neuron output o_i is given by a hyperbolic tangent (tanh) transfer function $o_i = \tanh(a_i) = \frac{2}{1+e^{-2a_i}} - 1$. W_{ij} is the synaptic strength[3] of the connection from neuron j to neuron i.

The two neurons $H_{0,1}$ of the CPG are fully connected with the four synapses $W_{00}, W_{01}, W_{10}, W_{11}$ and can form an oscillator if the weights are chosen according to an SO(2)-matrix:

$$\mathbf{W} = \begin{pmatrix} W_{00} & W_{01} \\ W_{10} & W_{11} \end{pmatrix} = \alpha \begin{pmatrix} cos(\varphi) & sin(\varphi) \\ -sin(\varphi) & cos(\varphi) \end{pmatrix}, \qquad (1)$$

with $-\pi < \varphi < \pi$ and $\alpha > 1$, the oscillator generates sine-shaped periodic outputs $o_{0,1}$ of the neurons $H_{0,1}$ (Fig. 4(b)) where φ defines a frequency of the output signals. In order to achieve stable locomotion (or stepping pattern), we here set φ to 0.5 and α to 1.01 and use a CPG postprocessing unit to shape the CPG

[3] This CPG model will show chaotic dynamics if its synaptic weights are set to $W_{00} = -5.5, W_{01} = 1.48, W_{10} = -1.65, W_{11} = 0.0$ with additional bias terms ($B_0 = -5.73, B_1 = 0.25$) projecting to the neurons H_0 and H_1, respectively. The chaotic pattern proves behaviorally useful for, e.g., self-untrapping from a hole in the ground [26].

signals. The resulting signals $M_{TC,CT,FT}$ drive the motors of the leg (Fig. 4(c)). With this setup, the neural controller acts as an open-loop controller to control the leg. We use this nonadaptive control setup to observe stepping performance of the leg with different foot structures on different terrains.

Efficient locomotion on different terrains

Here, we investigate locomotion efficiency of the leg with the bio-inspired tarsus on different terrains. We use specific resistance or cost of transportation (COT) [27] as means for evaluation and compare it with the other foot structures (i.e., the triangular tarsus and the standard hemispherical foot, see also Fig. 2). Two terrains were used: uneven terrain (rocky) and curved terrain (a cylindrical tube). The leg was attached to a moving cart which was constrained by two rails. This is to ensure that the leg moves along the terrains (Fig. 5) during locomotion. The specific resistance is the ratio between the consumed energy and the transferred gross weight times the traveled distance: $\epsilon = \frac{E}{mgd}$, where E is energy which is electric power consumption P of all motors of the leg multiplied by time t, mg is the weight of the dung beetle leg system including the cart (34.3 N), and d is the traveled distance (60 cm). Low ϵ corresponds to highly energy-efficient walking.

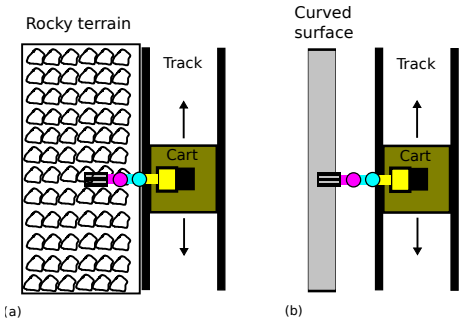

Fig. 5 The setup of the dung beetle-like leg with a cart to investigate locomotion efficiency on rocky terrain (a) and a cylindrical tube with a diameter of 8 cm (b).

Figures 6(a) and (b) give a comparison of specific resistances of the leg with the different foot structures during locomotion on the rocky terrain and the tube. The result shows that using the bio-inspired tarsus leads to low specific resistance, thereby highly energy-efficient locomotion compared to those with the triangular tarsus and with the standard hemispherical foot. In addition, during the experiments, the leg with the bio-inspired tarsus never failed to complete the track within a given time while the leg with the triangular tarsus and the standard foot failed several times. This is because the bio-inspired compliant tarsus can increase the contact area between the leg and the surface (Figs. 6(c) and (d)); thereby enhancing locomotion. We encourage readers to see a video showing locomotion of the leg with the bio-inspired compliant tarsus on the rocky terrain and the tube at
http://www.manoonpong.com/DB/S2.mp4.

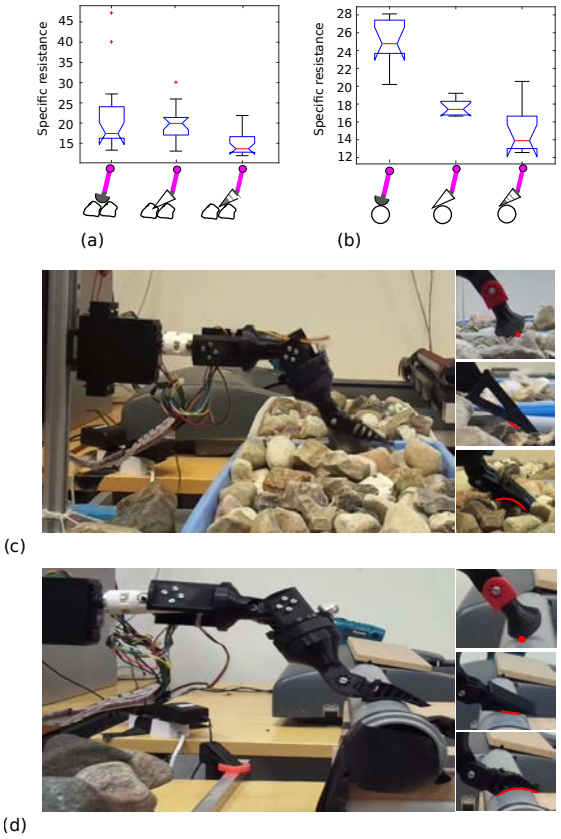

Fig. 6 (a) A comparison of specific resistances of the leg with the different foot structures during locomotion on rocky terrain. (b) A comparison of specific resistances of the leg with the different foot structures during locomotion on an 8-cm diameter tube. Each specific resistance plot was calculated from five successive experiments. (c) Experimental set-up of the leg system for locomotion on rocky terrain. Small figures show the contact areas, highlighted in red, between the surface and the different types of foot. (d) Experimental set-up of the leg system for locomotion on the tube. Small figures show the contact areas, highlighted in red, between the surface and the different types of foot.

4 Neural control with synaptic plasticity for adaptive locomotion

To enable the leg to autonomously adapt its stepping frequency to deal with environmental changes, we ex-

tend the CPG-based neural control (Fig. 4(a)) by introducing the third neuron H_2 (Fig. 7(a)). The neuron receives (preprocessed) sensory feedback P through the plastic synapse W_{2P} and connects to the control through the other plastic synapses $W_{02,20}$ (shown in red in Fig. 7(a)).

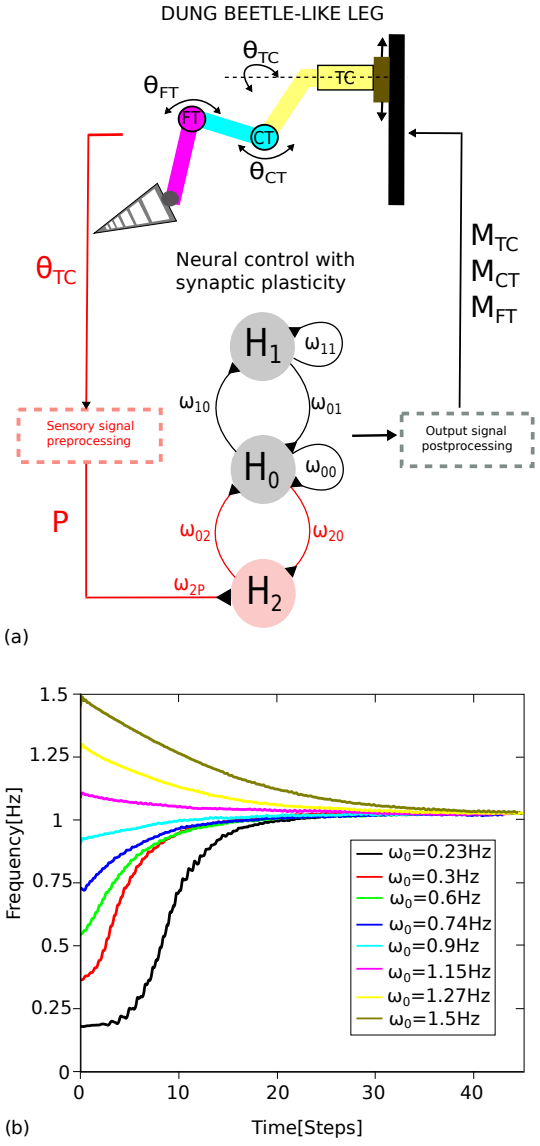

Fig. 7 (a) CPG-based neural control with synaptic plasticity for adaptive locomotion of the dung beetle-like leg. This adaptive neural control consists of the three neurons $H_{0,1,2}$ in total. Here, it receives the preprocessed TC-joint angle signal P provided by a sensory signal processing unit. We use a low pass filter to remove sensory noise at the processing unit. The outputs $o_{0,1}$ of the adaptive neural control are translated into proper motor commands at an output signal postprocessing unit. Red components are additional parts introduced to the original CPG-based neural control (Fig. 4 (a)). (b) Time series of the frequency changes during stepping in the air of the dung beetle-like leg for different initial frequencies ω_0. In all cases, the predefined phase shift $\Delta\phi$ set is set to 0.2π.

For our setup here, we use the TC-joint angle signal θ_{TC} of the leg as our sensory feedback P. The plastic synapses are governed by Hebbian-type learning rules based on correlation and relaxation terms driving the weights towards given relaxation values ($W_{1,2,3}$). The parameters a, $b > 0$ determine the influence of the individual terms [28]:

$$W_{2P}(t+1) = W_{2p}(t) + aP(t)o_2(t) - b(W_{2p}(t) - W_1) \quad (2)$$
$$W_{02}(t+1) = W_{02}(t) - ao_0(t)o_2(t) - b(W_{02}(t) - W_2) \quad (3)$$
$$W_{20}(t+1) = W_{20}(t) - ao_2(t)o_0(t) - b(W_{20}(t) - W_3) \quad (4)$$

The parameter φ of Eq. 1 is adapted based on the following frequency adaptation rule:

$$\varphi(t+1) = \varphi(t) + \eta W_{02}(t)o_2(t)W_{01}(t)o_1(t), \quad (5)$$

where η is a learning rate. o_1 and o_2 are the outputs of the neurons $H_{1,2}$, and W_{01} and W_{02} are synaptic weights (Fig. 7(a)). With an appropriate choice of the control parameters [28], the CPG-based control governed by above equations is able to autonomously adapt its internal frequency to the sensory feedback θ_{TC}. Here the control parameters are empirically set to $W_1 = 0.03$, $W_2 = 1$, $W_3 = 0$, $a = 1.0$, $b = 0.01$, and $\eta = 1.0$. As soon as the controller has adapted to the external frequency of the feedback, the average correlation of o_2 (sensory feedback) and o_1 (controller output) is equal to zero. After adaptation, the feedback can be removed from the controller while it maintains to oscillate at the adapted frequency. According to the hardware setup of the leg, a certain phase shift $\Delta\phi$ between the sensory feedback and the controller outputs occurs. This leads to instability of the adaptation process. Thus, we introduce a mechanism to compensate the delay (i.e., output signal postprocessing). It is given by:

$$s_0(t) = zcos(\Delta\phi_{set})o_0(t) + zsin(\Delta\phi_{set})o_1(t), \quad (6)$$

where $s_o(t)$ is a combination of H_0 and H_1 which is then processed to generate motor commands. The constant factor z is for adjusting the amplitude of the signal $s_0(t)$. $\Delta\phi_{set} \in [0, 2\pi]$ acts as a phase shift compensator which can be also used to obtain any desired phase relation. By driving the joints of the leg with the motor commands $M_{TC,CT,FT}$ proportional to $s_0(t)$ and feeding back the actual TC joint angle, the frequency adaptation process (Eq. 5) stably converges at a stepping frequency at which the angle signal θ_{TC} is delayed by a phase shift $\Delta\phi$ compared to the command M_{TC}.

Figure 7(b) shows the frequency adaptation process of the adaptive neural control, we set the phase shift

$\Delta\phi$ set between the TC-angle feedback and the motor command of the TC-joint to 0.2π and started the control at different frequencies. It can be seen that after a few seconds the adaptation process stably converges to a certain frequency which allows the leg to perform a proper stepping motion with respect to its biomechanical properties (i.e., structure, mass, motor torque, etc.). Note that different initial frequencies are defined by initializing different values of the synaptic weights $W_{00,01,10,11}$ of the control.

Adaptive locomotion on different treadmill speeds

Here, we investigate adaptive locomotion of the dung beetle-like leg with the bio-inspired compliant tarsus by performing the following procedure. At the beginning, we suspended the leg to let it step in the air and then placed it on a treadmill at a speed of 0.23 m/s. Afterwards, we increased the speed of the treadmill to 0.29 m/s and finally again suspended the leg in the air. Figure 8 shows the changes of the CPG internal frequency and the four plastic synapses with respect to the different situations. It can be seen that the controller can quickly react and adapt its output frequency to generate proper stepping behavior. We encourage readers to see a video showing another test of leg adaptation for different situations at
http://www.manoonpong.com/DB/S3.mp4.

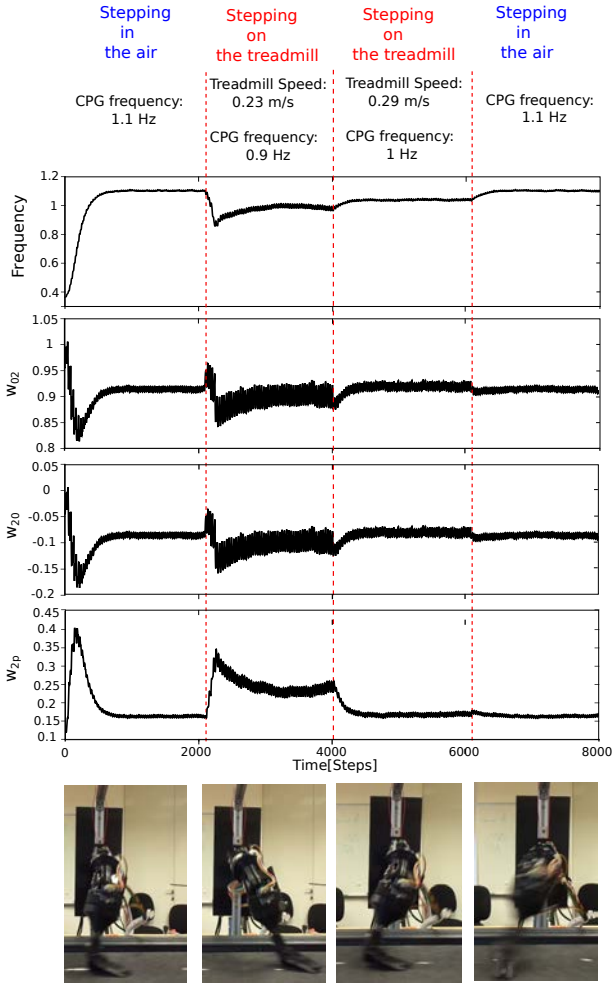

Fig. 8 Online frequency adaptation of the adaptive neural control for three different situations: Stepping in the air, stepping on the treadmill with a speed of 0.23 m/s and stepping on a treadmill with a speed of 0.29 m/s. The first plot shows the changes of stepping frequency with respect to the speed of the treadmill. The second, third, and forth plots show the changes of the plastic synapses $W_{02,20,2P}$. Bottom snapshots exemplify the leg movement on the treadmill.

5 Conclusions

In this study, we described the development of a whole dung beetle-like leg system from biological investigation to biomimetic construction and control. We analyzed the morphology of a real dung beetle by using μCT scans to obtain a 3D computer model. As a first step, here we focused only on the hind leg of the beetle for the conceptual design of a robot leg. The structures of the robot leg having the same proportion to the beetle leg were printed using a 3D printer. The robot leg was equipped with three active joints for moving the leg and potentiometer sensors for detecting the actual joint angle positions. A bio-inspired compliant tarsus (i.e., robot foot) was developed and attached to the last segment of the leg. Despite different foot structures have been developed and implemented on walking robots [6], [7], [8], [9], [10], [11], they are different and do not exhibit the passive compliance and the flexible structure that can increase the contact area between legs and substrate for efficient locomotion as shown here. The strategy of exploiting the properties of compliant materials and flexible structures to enhance locomotion behavior without complex control is considered as part of morphological computation [29].

Complementing the morphological computation, we used neural computation for locomotion generation and adaptation. Neural CPG-based control was employed for basic pattern generation of the leg and extended with synaptic plasticity for fast adaptation. Experiments show that 1) the compliant adaptable tarsus enhances locomotion of the leg compared to two other foot structures including a widely used hemispherical foot and 2) a combination of the proper biological-like structure (i.e., morphological computation) with the corresponding self-adaptive neural control (i.e., neural computation) results in proper motion behaviors and fast adaptability of the leg to changing locomotory situation. In

the next step, we will develop a complete dung beetle-like robot based on the leg and the compliant tarsus where each leg will be driven by the neural CPG-based control with synaptic plasticity. We will use local sensory feedback mechanisms for leg coordination and gait generation [30]. Furthermore, we will extend the neural control for object manipulation and transformation.

Acknowledgements This research was supported by Center for BioRobotics (CBR) at University of Southern Denmark (SDU, Denmark) and the Scandinavian Guest Professorship program of Kiel University (CAU, Germany).

References

1. Schneider A, Paskarbeit J, Schilling M, Schmitz J (2014) HECTOR, a bio-inspired and compliant hexapod robot. In: Proceedings of the 3rd Conference on Biomimetics and Biohybrid Systems, Living Machines 2014, pp 427-430
2. Roennau A, Heppner G, Nowicki M, Dillmann R (2014) LAURONV: A versatile six-legged walking robot with advanced maneuverability. In: Proceedings of the 2014 IEEE/ASME International Conference on Advanced Intelligent Mechatronics (AIM), pp 82-87
3. Manoonpong P, Parlitz U, W$\ddot{o}$rg$\ddot{o}$tter F (2013) Neural control and adaptive neural forward models for insect-like, energy-efficient, and adaptable locomotion of walking machines. Frontiers in Neural Circuits 7:12 DOI: 10.3389/fncir.2013.00012
4. Lewinger WA, Branicky MS, Quinn RD (2005) Insectin-spired, actively compliant hexapod capable of object manipulation. In: Proceedings of the 8th Int. Conf. on Climbing and Walking Robots (CLAWAR 2005), pp 65-72
5. Cruse H (1976) The function of the legs in the free walking stick insect, Carausius morosus. Journal of Comparative Physiology 112(2):235-262
6. Ohtsuka S, Endo G, Fukushima E, Hirose S (2010) Development of terrain adaptive sole for multi-legged walking robot. In: Proceedings of IEEE Int. Conf. on Intelligent Robots and Systems (IROS), pp 5354-5359
7. Bartsch S, Birnschein T, Cordes F, K$\ddot{u}$hn D, Kampmann P, Hilljegerdes J, Planthaber S, R$\ddot{o}$mmermann M, Kirchner F (2010) Spaceclimber: Development of a six-legged climbing robot for space exploration. In: Proceedings of the 41st International Symposium on and 6th German Conference on Robotics (ROBOTIK), pp 1-8
8. Tedeschi F, Carbone G (2014) Design issues for hexapod walking robots. Robotics 3(2):181-206
9. Walas K (2013) Foot design for a hexapod walking robot. Pomiary Automatyka Robotyka 17(193):283-287
10. Palmer LR, Diller ED, Quinn RD (2010) Toward a rapid and robust attachment strategy for vertical climbing. In: Proceedings of IEEE Int. Conf. on Robotics and Automation (ICRA 2010), pp 2810-2815
11. Voigt D, Karguth A, Gorb SN (2012) Shoe soles for the gripping robot: Searching for polymer-based materials maximising friction. Robotics and Autonomous Systems 60: 1046-1055
12. Bartsch S, Planthaber S (2008) Scarabaeus: A walking robot applicable to sample return missions. In Research and Education in Robotics EUROBOT 2008, pp 128-133
13. Heppner G, Buettner T, Roennau A, Dillmann R (2014) Versatile - high power gripper for a six legged walking robot. In: Proceedings of the 8th Int. Conf. on Climbing and Walking Robots (CLAWAR 2014), pp 461-468
14. Gladun D, Gorb SN (2007) Insect walking techniques on thin stems. Arthropod-Plant Interactions 1:7791
15. Philips TK, Pretorius E, Scholtz CH (2004) A phylogenetic analysis of the dung beetles: (Scarabaeinae: Scarabaeidæ): Unrolling an evolutionary history. Invertebrate Systematics 18:1-36
16. Halffter G, Halffter V, Favila ME (2011) Food relocation and the nesting behavior in scarabaeus and kheper (coleoptera: Scarabaeinae). Acta Zoologica Mexicana 27(2):305-324
17. Dai Z, Gorb SN, Schwarz U (2002) Roughness-dependent friction force of the tarsal claw system in the beetle Pachnoda marginata(Coleoptera, Scarabaeidae). Journal of Experimental Biology 205:2479-2488
18. Vagts S, Haschke H, Schlattmann J, Kleinteich T, Busshardt P, Pullwitt T, Gorb SN (2013) Towards understanding frictional properties of articular joints in beetle legs: μCT-based 3D model and multibody simulation of joint kinematics. In: Proceedings of 5th World Tribology Congress ISBN 978- 88-908185-09
19. Frantsevich L, Gorb SN (2004) Structure and mechanics of the tarsal chain in the hornet, Vespa crabro (Hymenoptera: Vespidae): Implications on the attachment mechanism. Arthropod Structure and Development 33: 77-89
20. Gladun D, Gorb SN, Frantsevich LI (2009) Alternative tasks of the insect Arolium with special reference to Hymenoptera. In: Gorb, S.N. (Ed.) Functional surfaces in biology - Adhesion related phenomena. Vol. 2., pp. 67-103
21. Ijspeert AJ (2008) Central pattern generators for locomotion control in animals and robots: A review. Neural Networks 21:642-653
22. Matsuoka K (1985) Sustained oscillations generated by mutually inhibiting neurons with adaptation. Biological Cybernetics 52:367-376
23. Buchli J, Righetti L, Ijspeert AJ (2006) Engineering entrainment and adaptation in limit cycle systems : From biological inspiration to applications in robotics. Biological Cybernetics 95(6):645-664
24. Yu J, Tan M, Chen J, Zhang J (2014) A survey on CPG inspired control models and system implementation. IEEE Transactions on Neural Networks and Learning Systems 25(3):441-456
25. Pasemann F, Hild M, Zahedi K (2003) SO(2)-networks as neural oscillators. In: Proceedings of the 7th International Work-Conference on Artificial and Natural Networks, pp 144-151
26. Steingrube S, Timme M, W$\ddot{o}$rg$\ddot{o}$tter F, Manoonpong P (2010) Self-organized adaptation of simple neural circuits enables complex robot behavior. Nature Physics 6:224-230
27. Gabrielli G, von Karman T (1950) What price speed?: Specific power required for propulsion of vehicles. Mechanical Engineering, ASME 72:775 781
28. Nachstedt T, W$\ddot{o}$rg$\ddot{o}$tter F, Manoonpong P (2012) Adaptive neural oscillator with synaptic plasticity enabling fast resonance tuning. In: Proceedings of Int. Conf. on Artificial Neural Networks (ICANN2012), LNCS 7552, pp 451-458
29. Pfeifer R, Iida F, Gomez G (2006) Morphological computation for adaptive behavior and cognition. Int. Congr. Ser. 1291, pp 22-29
30. Barikhan SS, W$\ddot{o}$rg$\ddot{o}$tter F, Manoonpong P (2014) Multiple decoupled cpgs with local sensory feedback for adaptive locomotion behaviors of bio-inspired walking robots. In: Proceedings of Simulation of Adaptive Behavior (SAB2014), LNAI 8575, pp 65-75